J Comp Physiol A (1984) 155:495–505

Journal of Comparative Physiology A Sensory, Neural, and Behavioral Physiology

The aerodynamics and sensory physiology of range fractionation in the cercal filiform sensilla of the cricket *Gryllus bimaculatus*

Tateo Shimozawa and Masamichi Kanou
Division of Behavior and Neurobiology, National Institute for Basic Biology, Okazaki, and Zoological Institute, Faculty of Science, Hokkaido University, Sapporo 060, Japan

Accepted July 23, 1984

Summary. 1. The deflection amplitude of cercal filiform hairs of different lengths was determined for various frequencies of air-current (Fig. 4). The angle threshold of the sensory neuron was then determined (Fig. 7). Both the deflection amplitude and angle threshold were length dependent.

2. In order to estimate the hair deflection, the spring stiffness of the hair supporting apparatus was measured. The stiffness varies by 10^2 depending on the hair length (Fig. 1).

3. Based on the mechanical properties measured, the deflection amplitude of hair in the sinusoidal air-current is estimated by means of a numerical solution of the equation of motion. The effect of the boundary layer due to the viscosity of air was taken into account. Long filiform hairs deflect more sensitively than short ones in the frequency range below 100 Hz (Fig. 4).

4. We compared a theoretical estimation of hair deflection with direct observation under relatively strong stimuli. The estimation and the observation are in good agreement (Fig. 5).

5. By using the estimated value of hair deflection and the sensory threshold (Shimozawa and Kanou 1984), we were able to determine the angle threshold of the sensory neuron. The angle threshold determined is 0.002° in long filiform hairs. In addition to this low angle threshold, sensory neurons with sensitivity only to fast deflection but not to slow deflection were revealed in association with the short filiform hairs (Fig. 7).

6. When oscillating, the filiform hairs show a self-damping property. The spring stiffness seems to be optimized in relation to the length and moment of inertia to give a critical-damping condition (Table 1).

7. The hair length, the spring stiffness, and the rate of relaxation of sensory neuron show a specific combination in a single sensillum. The specific combination underlies the range fractionation of the filiform sensilla.

Introduction

Seven cercal interneurons sensitive to air-current have been identified in the cricket *Gryllus bimaculatus* (Kanou and Shimozawa 1984). Each interneuron has a different frequency-threshold curve when measured by a sinusoidally alternating air-current. Interneurons 10-2 and 10-3 are velocity sensitive. Interneurons 8-1 (MGI), 9-1 (LGI), and others are acceleration sensitive.

We describe a wide variety of cercal filiform hair length in the companion paper (Shimozawa and Kanou 1984). The sensory threshold varies with the length of the hair (Figs. 4 and 5 in the companion paper). The short hairs are acceleration sensitive and the long ones are velocity sensitive. The cercal sensory afferents are thus range fractionated depending on the hair length. Interneurons with different properties receive sensory inputs from a specific group of the range fractionation.

The cercal hairs are driven principally by a kind of drag-force of the air-current (Tautz 1979). The viscosity of air gives not only the driving force to the hair but also a stagnating force to the air-mass on the cuticular substrate. In aerodynamics this stagnating air-mass is called the boundary layer.

The surface of the cercal floor is covered with a mat of dense cuticular villi (Shimozawa and Kanou 1984). This kind of microscopic roughness holds the air-mass effectively on the cuticular surface. The film of stationary air-mass on the surface

provides the no-slip condition required for all theoretical aerodynamics. This condition allows us to calculate the theoretical form of boundary layer even for a relatively small-sized object. The thickness of the boundary layer varies with the frequency of the air-current. It is of the order of 200–2,000 μm for a frequency of 100-1 Hz (Fig. 2).

The length of cercal filiform hairs varies between 30 μm and 1,500 μm (Dumpert and Gnatzy 1977; Shimozawa and Kanou 1984). The range of hair length overlaps with the depth of boundary layer at frequencies between 1 and 100 Hz. The thickness of the boundary layer on the cercus therefore has an important role to play in the range-fractionation of the sensory afferent.

The mechanisms underlying the range-fractionation are interesting. In order to separate the physiological properties of the sensory neurons of filiform hairs from the mechanical ones, it is preferable to measure the hair displacement. However, the angular displacement of the hairs to air-current stimulus at the threshold was too small to measure. The angular displacement must therefore be estimated theoretically from those mechanical properties which are measurable.

In this paper, we propose to show, (1) the measurement of spring stiffness which supports a filiform hair in the air; (2) a theoretical estimation of hair deflection to sinusoidal air-current stimulus; (3) an estimation of the angle threshold at which the sensory cell of the hair shows a spike discharge.

The analysis reveals that range fractionation in the cercal sensory afferent results from a combination of the aerodynamic and mechanical properties of filiform hairs and also from the relaxation rate of the sensory neuron.

Material and methods

Measurement of the stiffness of the hair supporting spring. The stiffness of the spring diaphragm which supports the shaft of a filiform hair is given by the ratio of the amount of torque applied to the hair to the resultant angular displacement. The gravity force was used to give a known amount of torque on the hair shaft (Fig. 1 B). A freshly dissected cercus was pinned to a vertical cork-board fixed under a horizontal microscope. The microscope had an ocular reticle which permitted us to measure the angle of a hair relative to the cuticular floor. The whole microscope, plus the preparation, was rotatable in a vertical plane.

A small sphere of poly-methylmethacrylate (Methacrylic Acid Methyl Ester Polymer, $n=7{,}000$–$7{,}500$, Tokyo Kasei) of 20–80 μm in diameter was used as a weight to give a delicate amount of gravity force. A weight sphere attached to a tungsten needle was transferred to a hair at an appropriate distance from the base. If filiform hairs come in contact with another object they exhibit an electrostatic or some other kind of cohesive force. If the tip radius of the needle is smaller than the hair radius, the cohesive force enables the sphere to hold on to the hair. No dislocation was observed during the microscope rotation.

The weight-loaded hair was first adjusted to a horizontal position, and the relative angle to the floor was recorded. The whole microscope and preparation was then rotated upside down, and the difference of hair angle (θ in Fig. 1 B) was measured.

As the socket wall may limit the true deflection, the size of the sphere and the distance from the base were chosen so as to cause an angular displacement (θ) smaller than 12° (0.21 rad).

The mass of the weight sphere is given as $m=4\ \pi\ \rho\ r^3/3$ (kg), where ρ is the density of methylmethacrylate ($=1.2\times10^3$ kg/m^3) and r is the radius of the sphere. The mass ranged between 4×10^{-11} and 2.6×10^{-9} kg. When this weight is attached at a distance of l (m), the moment torque around the hair base is given as $N_1=l\cdot m\cdot g$ (N·m), where g is the gravity acceleration ($=9.8$ m/s^2). The torque due to the self-mass of the hair was estimated. Assuming the hair to be a simple solid cone with length: L and basal radius: a, the mass is given as $M_h=\pi\ \rho_c\ a^2\cdot L/3$, where ρ_c is the density of the cuticular material ($=1.1\times10^3$ kg/m^3, Jensen and Weiss-Fogh 1962; Tautz 1977). The virtual center of the mass is located at a distance of $L/4$ from the conical base. The torque due to the self-mass is given by $N_h=M_h\cdot L\cdot g/4$. As a result of reversing the direction of the roque, the angular displacement θ (rad) is brought about by $N=2\ (N_1+N_h)$. The stiffness of the spring is therefore $S=N/\theta$ (N·m/rad). The gravity force due to the self-mass of hair caused no measurable angular displacement; the measurement resolution was 0.8°.

The cercus was placed at the bottom of a tube of 40 mm high and 10 mm diameter. The tube was necessary to attenuate the hair fluctuation due to atmospheric air-currents.

A numerical solution of the equation of the motion of the hair. The angular deflection of filiform hair during the air-current stimulus is described as a second-order differential equation (see Results). The equation contained an integration of torque along the longitudinal axis of the hair. The torque is represented by non-linear terms of angular velocity. Only a numerical solution was therefore possible. The second-order differential equation was decomposed into a pair of simultaneous first-order differential equations. The numerical solution was obtained by the Runge-Kutta method. The calculating step was 1/20 of a given period of time. This period is a reciprocal of the natural frequency of the hair or the stimulus frequency, whichever is the smaller. The natural frequency was estimated after an appropriate linearization of the equation (see Results). A microcomputer (Fujitsu FM-8) was used for the computation after a programming by F-BASIC. The integration of torque along the hair axis was performed by Simpson's approximation with a step of 1/30 of the hair length. It took about 30 s to obtain one value of deflection. Only a limited number of representative cases were computed. The cases comprised a combination of hair length L: 1,000, 500, 250, 100 μm, peak velocity of the sinusoidal air-current stimulus V_0: 100, 10, 1, 0.1 mm/s and frequency of the stimulus f: 1, 3, 10, 30, 100, 300, 600, 1,000 Hz.

Direct observation of the angular displacement. The amount of hair deflection in response to air-current stimulus was measurable in limited cases. Under a microscope a relatively long hair was chosen, and a dark field illumination was so adjusted as to obtain a bright reflection of light from the hair shaft. When the hair was exposed to a strong, high frequency, e.g. 50 Hz, air-current, the amplitude of hair shaft oscillation was visible

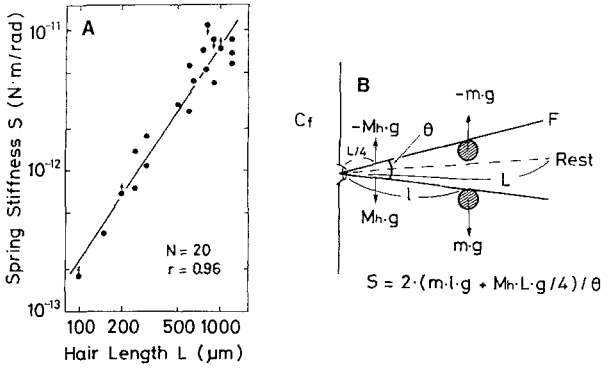

Fig. 1 A, B. Spring stiffness of hair supporting cuticle. **A** Stiffnesses of 20 different hairs in relation to hair length. Abscissa: hair length in logarithmic scale; upward arrows: minimum estimates due to resolution limit of angle measurement; dawnward arrows: maximum estimates due to a suspected probable limit by the socket wall. **B** Scheme of measurement, hatched circles: weight mass attached to filiform hair (F); Cf Cuticular floor, Rest: resting position, L hair length; l arm length of moment, θ: angular difference due to the gravity in opposite directions ($m \cdot g$ and $-m \cdot g$), M_h: self-mass of hair

because of its retinal after-image effect. The minimum resolution of displacement amplitude at the hair tip was 9 μm. One half of the tip displacement divided by the hair length gave the angular displacement of the hair.

Results

The spring stiffness of the hair supporting apparatus

In order to estimate the amount of hair deflection to a stimulus, we have to know the mechanical properties of the hair as well as the viscous force that will give moment torque to the hair shaft. Among these mechanical properties, mass and moment inertia are calculable from the hair dimensions under an appropriate assumption (see below). The stiffness of the spring diaphragm which supports the hair in the air has previously been unknown. We measured the spring stiffness under a static condition.

A weight of small plastic resin particles was attached to a hair shaft and the deflection caused by the gravity force in the opposite direction was measured (Fig. 1 B). The spring stiffness is represented by a ratio, momentum torque/angular displacement. The stiffness measured varied with the hair length (Fig. 1 A). The longer the hair, the stiffer was the supporting spring.

A theoretical estimation of the hair deflection to air-current stimulus

After measurement of the spring stiffness, it is possible to obtain a numerical solution of the equation of motion of the hairs.

The equation of motion describing angular displacement θ of the filiform hair under an air-current stimulus is

$$I \cdot \frac{d^2\theta}{dt^2} + R \cdot \frac{d\theta}{dt} + S \cdot \theta = N$$

where I = moment of inertia of the hair, R = frictional resistance within the hair base, S = stiffness of the spring diaphragm (see above), and N = total moment torque that is turning the hair around the base. If we assume that the hair is a solid cone, I is given by a simple integration about the distributed moment of inertia. The integration resulted in

$$I = \pi \rho_c a^2 \cdot L^3/30$$

where ρ_c = density of the cuticle (see above), a = hair radius at the base, and L = hair length. This is also expressed as $I = M_h \cdot L^2/10$, where M_h = mass of hair (see above). As we have no means to estimate the value of internal resistance R it is therefore assumed to be zero for the sake of simplicity. If this is not accurate, the actual angular displacement and its frequency dependency should be smaller than that estimated below.

The representative values of a, L, I, and S used for the numerical computation are listed in Table 1. They are determined in Fig. 1 A of this paper

Table 1. Mechanical properties measured and estimated values characterizing the hair motion

Hair length L (m) $\times 10^{-6}$	Base radius a (m) $\times 10^{-6}$	Spring stiffness S (N·m/rad) $\times 10^{-12}$	Moment inertia I (kg·m^2)	f_0 (Hz)	μ_0 (l/s) $\times 10^3$	h_*	f_n (Hz)
1,000	4	8.5	2.0×10^{-18}	328	1.6	0.80	197
500	2.8	2.7	1.2×10^{-19}	753	3.5	0.73	514
250	1.5	0.8	4.4×10^{-21}	2,146	11.8	0.88	1,019
100	0.9	0.21	1.1×10^{-22}	6,953	30.3	0.70	4,593

f_0: resonant frequency; $2\pi f_0 = \sqrt{S/I}$; μ_0: frictional coefficient; $2\mu_0 = k_d \cdot (L^3/3)/I$; where $k_d \approx 2 \times 10^{-5}$ (N·s/m^2); h_*: damping factor; $h_* = \mu_0/\omega_0$, $\omega_0 = 2\pi f_0$; f_n: natural frequency; $f_n = f_0 \cdot \sqrt{1 - h_*^2}$

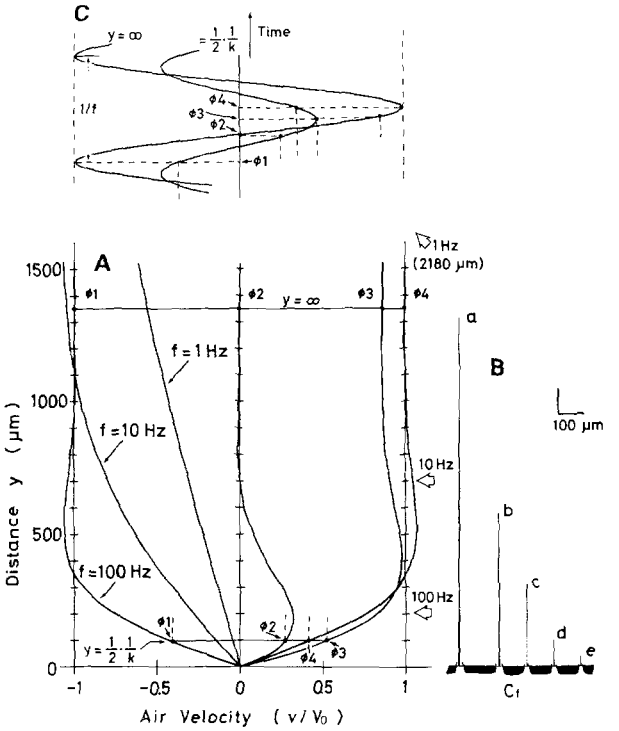

Fig. 2A–C. Thickness of boundary layer and length of cercal filiform hair. **A** velocity distribution of air oscillating in parallel to the substrate floor. Abscissa: instantaneous velocity normalized by peak-velocity of oscillation V_0, ordinate: distance from the substrate floor. Note attenuation and phase difference between in ($y=1/2k$) and out ($y=\infty$) of the boundary layer. $\phi 1$–$\phi 4$: corresponding instants of time (see **C**); open arrows, $1/k$ at indicated frequency; **B** cercal hairs drawn in common scale with **A**. Proportion of length to diameter is unity; *a–e*: hairs corresponding to those in Figs. 1A and 2A of the companion paper (Shimozawa and Kanou 1984); *Cf*: cuticular floor. **C** Time domain representation of attenuation and phase advance in boundary layer, ordinate: time in s; abscissa: common with **A**; other abbreviations: confer **A**

and Fig. 2 of the companion paper (Shimozawa and Kanou 1984).

Torque N is expressed in the complicated method of fluid dynamics. First, we have to clarify the air-particle velocity at various distances from the substrate. Second, we have to describe the amount of drag-force acting on a cylinder of an arbitrary diameter. Third, we need to calculate the drag-force due to the relative velocity between a part of a hair and the air-current. The product between this drag-force and the arm-length of moment gives a torque that turns the hair around the center of deflection (hair base). Fourth, the moment torque must be integrated along the length from the hair base to the tip.

The boundary layer. The theory of air motion produced by a smooth and infinitely large plate oscillating parallel to itself is known as Stokes's second problem (Schlichting 1979). After a slight modification of the coordinate system of this problem, we were able to derive the distribution of air-velocity neighboring on the cuticular surface. If we assume that an air-current far from the cuticular surface moves in parallel to the surface and with a velocity of $V_0 \cdot \cos(2\pi f \cdot t)$ (m/s), the instantaneous velocity v at a distance y (m) from the surface is expressed as follows.

$$v(y,t) = V_0 \cdot \exp(-k \cdot y) \cdot \cos(2\pi f \cdot t - k \cdot y) - V_0 \cdot \cos(2\pi f \cdot t) \quad \text{(m/s)}$$

where $k = \sqrt{\pi f / v}$ (m^{-1}), v = kinematic viscosity of air (1.5×10^{-6} m^2/s at 20 °C), V_0 = stimulus intensity, the peak velocity of sinusoidal air-current at a far distant location of y, f = alternating frequency, t = time in s.

The viscosity of air gives a stagnating force to the air-mass on the cuticular surface and results in an attenuation and a phase-advance of air-current velocity near the surface (Fig. 2A, C). The thickness of the boundary layer is of the order of $1/k$. The thickness decreases as the frequency increases (Fig. 2A). The value of $1/k$ is 2,180 μm for 1 Hz, 690 μm for 10 Hz, and 220 μm for 100 Hz. The short filiform hairs are buried in the boundary layer when the frequency is low (Fig. 2B).

Drag-force on the cylinder. The theoretical drag-force acting on a cylinder is given by Oseen's method of Stokes's approximation (Imai 1980). The drag-force per unit length of the cylinder caused by a steady air-current perpendicular to the cylinder axis is expressed as follows. Force

$$F(U, r) = 8\pi \cdot \eta \cdot U / (2 \cdot S + 1) \quad \text{[N/m]}$$

where $S = \ln(8/R) - \gamma$, R is the Reynolds number for cylinder radius ($= 2r \cdot U/v$), U is the air-current velocity (m/s), r is cylinder radius (m), η is the viscosity of air (1.82×10^{-5} N·s/m^2 at 20 °C), v is the kinematic viscosity of air (see above), γ is Euler's constant ($= 0.577$). In simple,

$$F(U, r) = 22.9 \cdot U / (1.72 - \ln(r \cdot |U|)) \quad \text{[N/m].}$$

Relative air-velocity responsible for hair motion. When a hair deflects, a small piece of the shaft at a distance y has a tangential velocity, $y \cdot d\theta/dt$, against the substrate floor (Fig. 3). The piece therefore experiences a wind whose velocity is a difference vector of $v(y, t)$ and $y \cdot d\theta/dt$ (open arrow in Fig. 3). In the present instance, it is sufficient to

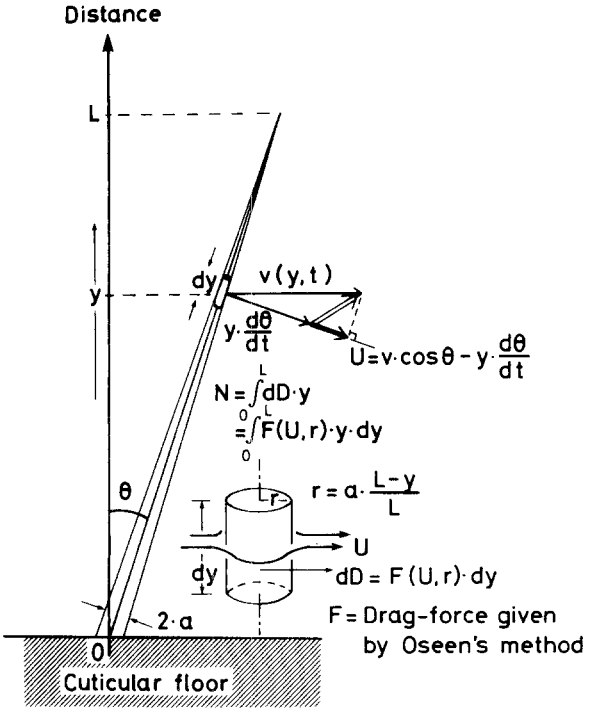

Fig. 3. Angular displacement, drag-force, and moment torque on hair. Vectors concerned with a small piece of hair shaft shown. y: distance from floor; $v(y, t)$: instantaneous velocity of air-current stimulus at y; θ: angular displacement; open arrow: wind vector actually faced on the piece; thick arrow: air-velocity component U causing drag-force; N: total turning torque; $2 \cdot a$: hair diameter at base; L: length of hair; Inset: dD: drag-force working on a cylinder of infinitesimal length dy; r: radius of hair shaft at y

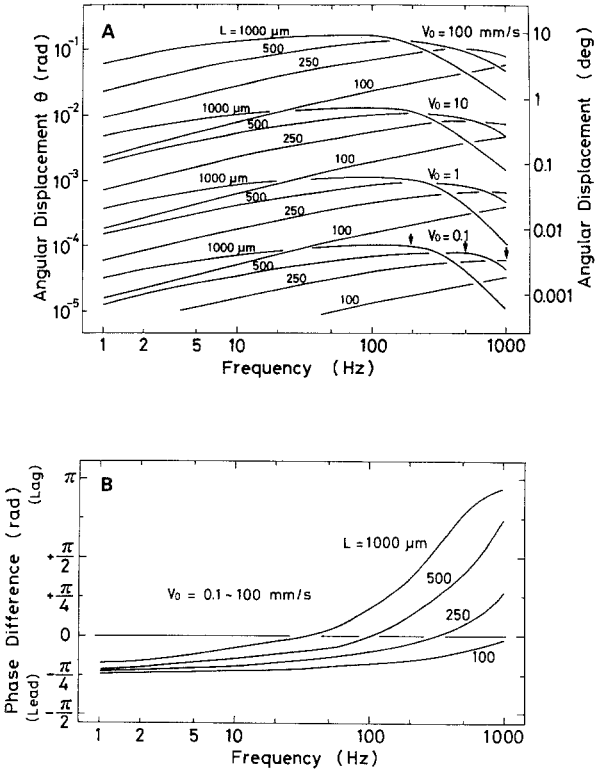

Fig. 4A, B. Hair deflections theoretically estimated under different conditions of hair length L and peak velocity V_0. **A** angular displacement of hair shaft in radian (rad) and degree (deg) on a logarithmic scale; Abscissa: frequency in logarithmic scale; downward arrows: natural frequencies of hair with indicated length. **B** Phase difference of hair deflection relative to velocity sinusoid of air-current

consider the velocity component perpendicular to the hair axis. The relative velocity U can therefore

$$= v \cdot \cos\theta - y \cdot \frac{d\theta}{dt} \quad \text{(thick arrow in Fig. 3).}$$

As θ is smaller than 10°, $\cos\theta \approx 1$, here

$$U = v - y \cdot \frac{d\theta}{dt}.$$

As we have already assumed that the hair is a solid cone with base diameter of $2a$, the radius r of the cylinder piece will be $a \cdot (L-y)/L$. The instantaneous values of drag-force F are now expressed with a variable y. The drag-force working on this infinitesimally small piece of hair can be expressed as

$$dD = F \cdot dy.$$

Total torque turning the hair around the base. A drag-force dD gives a turning moment to the hair shaft. The arm length of moment is y because of a small θ. The turning torque is $dD \cdot y$. The turning torque is distributed along the hair but works on a single axis of solid shaft. The integration of distributed torque along the length therefore gives total torque N (Fig. 3). The instantaneous values of N must be calculated successively at every step of the numerical solution of the equation of motion.

Figure 4A and B show the theoretical estimations of deflection amplitude and phase relation to the velocity sinusoid of air-current. A long hair is estimated to be more sensitive than a short one in the frequency range below 100 Hz. A hair with a length around 1,000 µm is estimated to be velocity-dependent because of the flat deflection-frequency curve in its range. In contrast to this, those less than 250 µm are estimated to be rather acceleration-dependent. However, their slopes are about 10 dB/decade change in frequency (dB/dec) rather than 20 dB/dec. A slope of 10 dB/dec is an indication of the effectiveness of the boundary layer thickness which varies with the order of $\sqrt{f}$.

At the lower frequencies, the hairs deflect in phase-advance by $\pi/4$ from the velocity sinusoid

(Fig. 4B). This results from the phase-advanced motion of air within the boundary layer (Fig. 2C). The fact that the viscosity causes a phase-advancement is somewhat paradoxical. Around the best frequencies, hairs deflect with a phase-lag between $\pi/4$ and $\pi/2$. At the frequencies higher than the natural frequency, the phase-lag increases and reaches π. At these frequencies, the physical constraint of the hair motion is the moment inertia, and the hair moves in anti-phase to stimulus. The deflection amplitude decreases sharply, 20 dB/dec, in the frequency above the natural frequency. The deflections of short hair are phase-advanced from those of long one. At 50 Hz, a 250 μm hair deflects in advance by 0.06–0.1 π from a 500 μm hair.

Although we took no account of the internal resistance, curves in Fig. 4A are rather flat and have no sharp resonance. This suggests that their aerodynamic system has a self-damping property.

A comparison of theoretical estimation with direct measurement

A theoretical estimation was compared with direct observations (Fig. 5). The direct measurement of angular displacement was limited for strong stimuli, for long hairs, and for high frequency, because of a resolution limit of microscopic measurement and the range of after image. The estimated values were in good agreement with the direct observations in several hairs of different lengths.

Figure 5 also indicates that the angular displacement of a hair increases with the stimulus intensity with the relation of $V_0^{1.08}$.

Optimal stiffness of the hair supporting spring

The non-linearity between stimulus velocity and angular displacement was estimated to be slight; the exponent is about 1.08 (Figs. 5 and 6). This is a reflection of the physical property of the drag-force; a graphical examination of the Oseen's formula (see above) resulted in a similar relation. Under the present conditions of cylinder radius r and air-current U (m/s), Oseen's drag force F (N/m) is practically expressed as $k_0 \cdot U^{1.08}$, where $k_0 = 3.8 \times 10^{-5}$ (N·s/m^2).

The first order approximation was obtained by the use of Taylor's expansion around appropriate values of U. In the range of U between 0.1×10^{-3} and 100×10^{-3} (m/s), it is plausible to express $F = k_d \cdot U$, where $k_d = 2 \times 10^{-5}$ (N·s/m^2). By this linearization, we were able to transform the equation of the motion of a hair into

$$I \cdot \frac{d^2\theta}{dt^2} + S \cdot \theta = \int_0^L k_d \cdot \left(v(y,t) - y \cdot \frac{d\theta}{dt} \right) \cdot y \cdot dy.$$

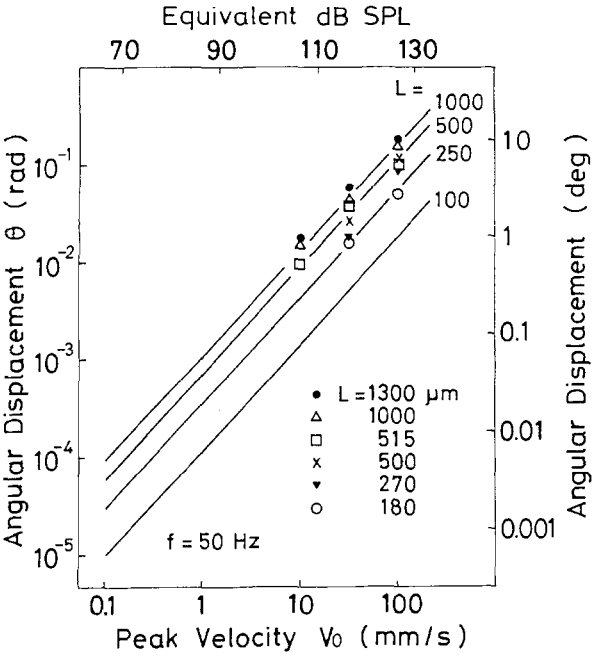

Fig. 5. Angular displacement θ plotted against stimulus intensity V_0 at 50 Hz. Solid lines: theoretical estimations, Parameter: hair length L, symbols: direct observations in 6 different hairs, Equivalent dB SPL: sound-pressure-level relative to 2×10^{-5} N/m^2 of free field wave which has the same air-particle velocity as stimulus intensity V_0, for the convenience of comparison

Because $d\theta/dt$ is independent on y, the right-hand half

$$= k_d \cdot \int_0^L y \cdot v(y,t) \cdot dy - k_d \frac{d\theta}{dt} \cdot \int_0^L y^2 \, dy.$$

The integration in the last term is $L^3/_3$. The equation thus becomes

$$I \cdot \frac{d^2\theta}{dt^2} + k_d \cdot \frac{L^3}{3} \cdot \frac{d\theta}{dt} + S \cdot \theta = k_d \cdot \int_0^L y \cdot v(y,t) \cdot dy.$$

The second term is a self-damping force due to the viscosity of the air, and the right most one is the driving term.

This linearization permits a qualitative analysis of hair motion. Assuming the simultaneous form of the equation to be

$$\frac{d^2\theta}{dt^2} + 2\mu_0 \cdot \frac{d\theta}{dt} + \omega_0^2 \cdot \theta = 0,$$

where

$$2\mu_0 = k_d \cdot (L^3/3)/I, \text{ and } \omega_0^2 = S/I.$$

μ_0 is the frictional coefficient, and ω_0 is the angular resonant frequency ($= 2\pi f_0$).

The values of resonant frequencies and frictional coefficients for hairs of different length were

Table 2. Best frequencies and maximum deflections in relation to the air-particle displacement and thickness of boundary layer

Hair length L (m)	Best frequency f_b (Hz) $V_0=100\sim0.1$ mm/s	Maximum deflection θ_M (rad) $V_0=100\sim0.1$ mm/s	Displacement ratio R_d	Length ratio R_l
$1{,}000\times10^{-6}$	70 – 200	1.5×10^{-1}– 1×10^{-4}	0.33–0.62	3.8–6.7
500	200 – 500	1.4×10^{-1}– 0.73×10^{-4}	0.36–0.57	3.2–5.1
250	500 – 1,000	1.0×10^{-1}– 0.63×10^{-4}	0.37–0.49	1.8–3.6

$R_d=d_h/d_a$, $d_h=\theta_M\cdot L$, $d_a=V_0/(\pi\cdot f_b)$, $R_l=L/(1/k)$, $1/k$: thickness of boundary layer
Values in left-hand side in each column for $V_0=100$ mm/s; for right-hand side values, $V_0=0.1$ mm/s

calculated and are listed in Table 1. The damping factors which best express the fidelity of the system were estimated (Table 1, h_*). All values of the damping factor h_* obtained were close to 0.71 ($1/\sqrt{2}$), which is known as the critical-damping condition of second order system. The stiffness of the hair-supporting spring and the hair length (or its diameter) are thus in an optimal condition of stability and frequency range. If a hair is supported by a spring stiffer than the one observed, the hair would be under-damped and would show a large deflection at a particular frequency of stimulus air-current.

Hairs under a strong stimulus have lower values of best frequency than those under a weak one (Fig. 4A, Table 2). This indicates that a hair moving with large velocity behaves as an over-damped system because of the non-linearity of the drag-force.

Air-particle displacement and hair-tip motion at the best frequency

Around the best frequency, the hair deflects with a phase difference, between $\pi/4$ and $\pi/2$, behind the velocity of the air-current (Fig. 4B). The air-particle displacement lags behind the velocity by $\pi/2$. The motion of the hair-tip is therefore roughly in-phase or slightly behind with the air-particle displacement. We examined whether the tip outruns the moving air-mass or not. By means of Fig. 4 we can determine the best frequency f_b and maximum angular displacement θ_M. These values vary with the stimulus intensity V_0. The amplitude of air-particle displacement is given as $V_0/(\pi\cdot f_b)$. This may be compared with the hair-tip displacement, $L\cdot\theta_M$ (Table 2). The displacement of hair-tip at the best frequency is about one half of the air-particle displacement at the tip (R_d in Table 2). Under any condition examined, the tip displacement never exceeded the air-particle displacement. Table 2 also presents the ratio between hair length and the thickness of the boundary layer at the best frequency (R_l). The maximum deflection occurs when the hair is 1.8–6.7 times long above the boundary layer.

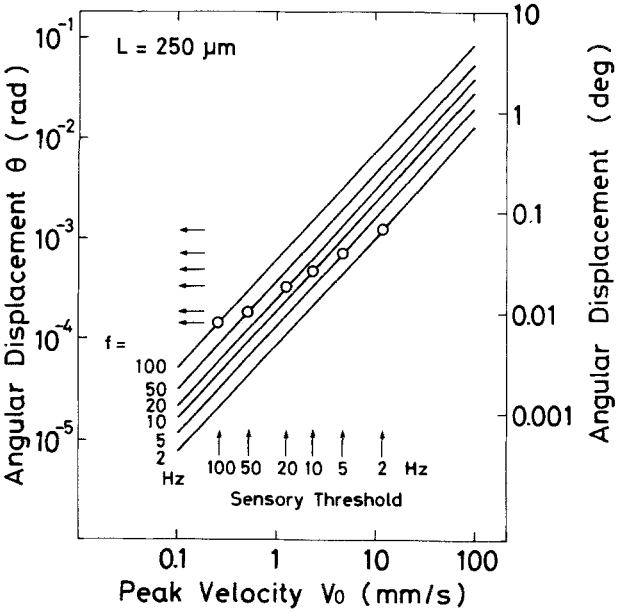

Fig. 6. An example of graphical determination of angle threshold. A particular case of 250 µm hairs indicated. Solid lines: theoretical estimations of hair deflection (ordinate) against air-current velocity (abscissa); parameter: frequency; upward arrows: sensory thresholds in velocity value (abscissa) at frequencies indicated; open circles: cross points of lines and upward arrows of the same frequency; horizontal arrows: ordinate values of open circles (angle thresholds to be read out)

Estimation of the angle threshold of the sensory neuron

Using the angular displacement estimated above, we were able to determine the amount of deflection angle of a filiform hair at the sensory threshold. The angle threshold was graphically determined (Fig. 6). For a hair of a certain length, the theoretical relations of angular displacement against the air-current velocity were drawn for a set of frequencies. The velocity thresholds of sensory hairs with different lengths are indicated in Fig. 7 of the

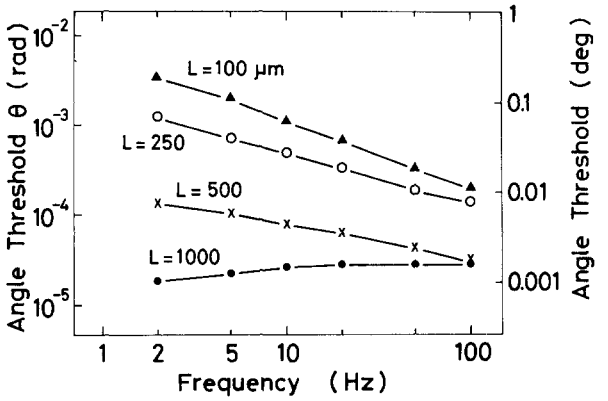

Fig. 7. Angle thresholds of filiform sensilla. L hair length. Note that the angle threshold is not necessarily constant but depends on rate of change: frequency (abscissa)

companion paper (Shimozawa and Kanou 1984). The sensory thresholds of each frequency were plotted on the abscissa (upward arrows in Fig. 6). Angular displacement at the threshold velocity gives the angle threshold at each frequency (horizontal arrows in Fig. 6).

The angle threshold determined was clearly dependent on both the length of hair and the frequency of deflection (Fig. 7). The sensory neuron of a long hair was estimated to elicit a response to a smaller deflection than a short one. The angle thresholds of long hairs were between 0.001 and 0.002° for frequencies from 2 to 100 Hz. In contrast to this, the short hairs were estimated to be less sensitive to angular deflection. In addition to the sensitivity difference, the angle threshold of short hair neurons showed a strong frequency-dependency. The angle threshold varies with a slope of 10–15 dB/dec. In other words, the sensory neuron of a short hair elicits a response only when the hair shaft deflects at a certain rate of change (0.6–6°/s) but not when the deflection is stationary.

Given these facts about the angle threshold, the difference must be attributed solely to sensory neurons. Filiform hairs of different lengths must therefore combine with a sensory neuron of different properties; the shorter the filiform hair, the less sensitive to slow deflection will be the sensory neuron associated with it.

Discussion

As a result of the present analysis, we can attribute the range fractionation in the cercal sensory afferents to the following factors: (1) the formation of a boundary layer which transforms the frequency of air-current to the thickness of the layer; (2) the length of the hair which acts as a mechanical filter selective to a certain depth of the boundary layer; (3) the rate of relaxation of the sensory neuron which transmits a response after the stimulation by the deflected hair.

In the present analysis, the boundary layer was calculated by the theory for a smooth and infinitely large plate. The stimulus air-current is moving in parallel to the body axis of the animal. The incident angle of air-current to the cercal axis is about 30°. The distribution of particle velocity around a cone shaped object to which a sinusoidal air-current obliquely passes is an extremely complicated physics and no exact solution is available, however, the stream lines around an ellipsoid of revolution placed obliquely in a steady flow are known (Schlichting 1979). The stream lines around the ellipsoid have a considerable amount of parallel component with its longitudinal axis when Reynolds number is small. Therefore the nominal size of the cercus is its length but not the radius. Even at the extreme case: air-current passing a cylinder perpendicularly to the long axis, the boundary layer formed above the cylinder surface can be approximated by the solution for an infinite plate, if the radius of cylinder is sufficiently large relative to the displacement amplitude of air particle (Schlichting 1979). The displacement amplitude of air-current stimulus is given by $V_0/\pi f$. The displacement amplitude is less than 1 mm when calculated for stimuli with parameters of 1 Hz and 3 mm/s, 10 Hz and 30 mm/s, 100 Hz and 300 mm/s, and so on. The higher the frequency or the lower the velocity, the displacement is the smaller. The length of cercus is sufficiently large compared to the displacement amplitude of air particle within the most range of stimulus used in the present analysis. On this point of view, the very left upper part of the frequency threshold curves shown in the companion paper (e.g. 1 Hz and 300 mm/s) and hairs at the tip of cercus are certainly out of range of the present analysis.

It is questionable whether the tall forest of filiform hairs itself affects the formation of boundary layer. Although the hairs are very long, the diameter of hair shaft is considerably small compared to the diameter and the length of cercus. The incident angle of air-current is perpendicular to the shaft. The displacement amplitude of air particle is comparable or larger than the hair diameter in the most range of stimulus (e.g. 100 μm at 10 Hz and 3 mm/s). This is the reason that we can calculate the drag-force acting on hair shaft by Oseen's method which is originally an approximation for steady flow past a cylinder. The boundary layer of a steady flow past a cylinder is given by the

same Oseen's method as follows (Imai 1980). Air current velocity at distance y from the center of cylinder placed in the steady flow with velocity U

$$u(y)=\frac{U}{2\cdot S+1}\cdot\left(\ln\frac{y^2}{a^2}-\frac{a^2}{y^2}+1\right)$$

where $S=\ln(8/R)-\gamma$, a is cylinder radius, R is the Reynolds number for cylinder radius ($=2a\cdot U/\nu$), ν is kinematic viscosity of air, γ is Euler's constant. The thickness of boundary layer varies with the cylinder diameter and flow velocity. The thickness estimated by Oseen's formula is about 10 to 20 folds of hair diameter at largest. Therefore the effect of hair on the air-current extends only up to 180 μm in the thickest hairs (9 μm in diameter), and 40 μm in the thinest ones (2 μm). When air is oscillating, the boundary layer is considerably thin compared to that in the steady flow (Schlichting 1979); see the fact that the boundary layer formed on the cercus for oscillating air-current is 2,200 μm at 1 Hz, 220 μm at 100 Hz and so on, in contrast to 10 mm or so estimated for the steady flow. The density of filiform hairs is rather sparse; inter-hair distance is about 100 μm or more at the cercal surface (Fig. 1 in the companion paper). Furthermore, the hairs project into the radial direction. Therefore the effect of a single hair on the air-current does not reach to the neighbouring hair. The sparse forest of thin filiform hairs does not affect the formation of boundary layer on the cercus.

The displacement amplitude of air-particle is about 0.3 μm at the stimulus of 100 Hz and 0.1 mm/s. Oseen's method is no more adequate for drag-force calculation at the higher frequencies. The very lower-right corner of the frequency threshold curves presented in the companion paper (Shimozawa and Kanou 1984) is a limit of the present analysis.

All theories of aerodynamics require two conditions: that the surface of solid object is smooth and that the air particles at the surface do not flow. The latter requirement is known as the no-slip condition. The surface smoothness and the no-slip condition are a priori assumed for the sake of mathematical simplicity. No physical basis exists for the conditions. It is evident that the smoothness and the no-slip condition are physically incompatible to each other. The smoothness of surface is not about the absolute extent of microscopic roughness but about the relative extent to the size of macroscopic shape of the object or to the thickness of boundary layer formed. The cercal floor is covered with a mat of cuticular villi (Shimozawa and Kanou 1984); the size of villi are 5 μm in height and 0.6 μm in diameter, and the inter-villus distances are about 2–3 μm. The mat of 5 μm thick is sufficiently smooth compared to the cercal shape with diameter of 1 mm and length of 10 mm. This is also true even compared to a 100 μm filiform hair. In contrast to this macroscopic smoothness, a microscopic boundary layer is formed around a villus. The boundary layers formed by each villus fuse because the inter-villus distances are shorter than the thickness of the layer (see above). The fused boundary layer, a film of stationary air-mass of 5 μm thick, satisfies the macroscopic requirement of no-slip condition. Although the presence of cuticular villi allows us to assume the no-slip condition for analysis, we don't know whether the no-slip condition is satisfied or not if the cercus has no such villi.

Filiform hairs ranging from 30–1,500 μm, exist in the cercus (Shimozawa and Kanou 1984). In addition to this variation, the spring stiffness of the hair supporting apparatus has a variation of about 10^2, and the relaxation rate of sensory neuron also varies by about 6 ($10^{0.75}$, see below). In spite of these variations, a single filiform sensillum has a specific combination of hair length, spring stiffness and sensory neuron. During the morphogenesis or ecdysis, the hair shaft and the spring diaphragm are secreted by two differentiated epithelial cells, the trichogen cell and the tormogen cell respectively (Gnatzy and Romer 1980). In a hemimetabolous insect, a set of one trichogen cell, a tormogen cell, a sensory neuron, and a neurilemma cell are differentiated from a single mother cell (Lawrence 1966). The specific combination of the hair length, the spring stiffness, and the type of sensory neuron observed in the cercal filiform sensilla is correlated with this common lineage. The major differentiation of the mother cell of the sensillum underlies the range fractionation.

Although it was inevitably necessary to intercalate a theoretical estimation, we were able to determine the angle thresholds of filiform sensilla. The determined angle was 0.002° for a long hair. This value is considerably smaller than that assumed by a previous worker: 0.1° (Tautz 1979). In addition to the low angle threshold in longer hairs, the distinct frequency-dependency of the angle threshold in shorter hairs was revealed. The sensory neuron of shorter hair is sensitive to the fast changing deflection but not to the steady deflection. Thus the neuron would show a phasic spike discharge after the onset of a steady hair deflection, if given. The phasic response to steady stimulus involves electrical inactivations in the membrane

and mechanical relaxations in the sensory transduction process. The sensory afferents of the present study respond to each cycle of the air-current stimulus (see the companion paper). Inactivation in the process between receptor potential and impulse initiation is therefore unlikely. We suspect that the rate-dependency of angle threshold is attributable to some mechanical properties of the sensory transduction structure. A viscoelastic relaxation or mechanical creep would occur in the tubular body of the sensory cilium when hair deflection is slow.

A similar kind of differentiation in the adaptation rate has been reported in the sensory neurons of a crayfish mechanoreceptor (Takahata 1981). In the crayfish neurons, differentiations are suggested not only in the electrical adaptation of the membrane but also in parts of the sensory transduction.

The fact that the cercal sensory neurons are not only sensitive to angular deviation of hair but some of them are sensitive to the speed of deviation has been pointed out by Petrovskaya et al. (1970). The present study reveals that the sensory cells accompanied with a long filiform hair are angle sensitive and those accompanied with a short one are sensitive to speed of deviation.

The directionalities of cercal filiform sensilla have been reported in the cockroach (Nicklaus 1965; Dagan and Camhi 1979), and in the cricket (Gnatzy and Tautz 1980). The sensillum is called either a *T*-(transverse to cercal axis) or an *L*-(longitudinal) hair depending on the preferential direction. In the present measurement of the spring stiffness, however, the directionality was not accounted for, because of the difficulty of discrimination, especially among short hairs. In spite of this uncertainty about the directionality, the stiffness showed a wide variation over 10^2 difference and a clear relationship with hair length. The mechanical polarization underlying the directionality, if any, can be estimated from the scattering range of the measured stiffness. The range is smaller than 2 (Fig. 1). A similar amount of mechanical polarization has been reported in cockroaches by Nicklaus (1965).

According to ultrastructural studies of the hair base (Gnatzy and Tautz 1980), hairs are supported by a cuticular diaphragm (joint membrane), and the first structure of the mechano-sensory transduction is a cuticular lever which compresses the tubular body of sensory cilium. The displacement of cuticular lever at threshold is less than 0.1 nm at largest, 3×10^{-5} radian multiplied by 1 μm as the possible longest lever arm. The measured spring stiffness is so delicate that the elasticity is compensated for on the critical-damping condition only by the air viscosity. Considering the delicate elasticity of the hair base and the unexpectedly high sensitivity to angular displacement, we suspect that the stiffness is a direct reflection of the elasticity of the tubular body and the surrounding wet structures, and that the tubular body is a kind of iso(volu)metric strain sensor rather than a sensitive displacement sensor.

The critical-damping condition in the cercal hair has been suggested by Petrovskaya et al. (1970), although the correlation with hair length has not been mentioned. The critical-damping condition is realized only by a specific combination of hair size and stiffness of supporting spring. The present study reveals the well-coupled specialization in a set of trichogen and tormogen cells in a common cell lineage comprising a single sensillum.

Gnatzy and Tautz (1980) reported that the best frequency of long, 800–1,000 μm cricket hairs was 100–200 Hz. The natural frequency estimated here for a 1,000 μm hair matches well with their values. This supports, though not proves, the validity of the present theoretical estimation in addition to providing agreement with direct measurements of the deflection to the intense stimuli.

The sensory afferent of a short hair responds in phase-advance by about 0.6 π compared to that of a long one at 50 Hz (Shimozawa and Kanou 1984). The theoretical phase difference in deflections between short and long hairs was 0.1 π at the frequency. Therefore the rest of phase-advancement, 0.5 π, must be attributed to the sensory neuron. When a sensory neuron shows a phasic response expressed by a power function of time, $B \cdot t^{-n}$, the linear transfer function is given by $C \cdot \varsigma^n$, where s is the Laplace operator (Chapman and Smith 1963). The meaning of ς^n is that the response is the nth order time-derivative of the stimulus wave form. The frequency domain expression of the transfer function is $D \cdot f^n \cdot \exp(j \cdot \pi/2 \cdot n)$. The response amplitude increases with frequency by the power of n and the phase-advance by $\pi/2 \cdot n$. The slope of frequency dependency of angle threshold in the short hair was 15 dB/dec. Therefore n is 0.75 (15/20) and the phase-advance of sensory neuron response from hair deflection is 0.4 (0.75/2) π. As a total, from air-current to afferent response, n is about 1 and phase-advance is about 0.5 π. The short hairs extract the first-order time-derivative of the stimulus quantity, in this case the acceleration.

A purely theoretical model of a mechanoreceptor hair has been offered by Fletcher (1978).

Fletcher's model states that the maximum displacement of the hair tip is twice that of the air-particle displacement at the best frequency. The hair-tip displacement of the thoracal mechanoreceptors of a lepidopteran caterpillar matched well to this model (Tautz 1977). An extensive study of the structure and mobility of the long filiform hair of the cricket *G. bimaculatus* (Gnatzy and Tautz 1980) shows, however, that the amplitude of the hair-tip at the best frequency is about one half of the air-particle displacement. Fletcher's model resulted in an over-estimation probably because the differential equations are inadequately linearized and the boundary layer is ignored. The theoretical estimations presented in Table 2 match well with the observations.

The range of hair length of optimally adapted hairs has been predicted to be 1.4–4.2 times that of the thickness of the boundary layer, $1/k$ (Fletcher 1978; Tautz 1979; our definition of the boundary layer thickness differs from theirs by a factor of $\sqrt{2}$). The length ratios given in Table 2 match well with the prediction. However, this ratio seems to vary with hair lengths. The longer the hair, the larger the ratio.

Another theoretical model offered by Henson and Wilkens (1979) neglected the effect of frequency on the thickness of the boundary layer and contained an incorrect formula (miscalculation or typographic error uncertain), therefore the results can not be compared.

Our theoretical estimation is based on the aerodynamics and the actual measurement of spring stiffness. Although this requires a tedious numerical computation, it succeeds in showing good agreements with actual observations in the best frequency and the displacement amplitude. The confirmed estimation reveals the low angle threshold which is otherwise impossible to measure, and various types of sensory neurons with different sensory adaptation.

Acknowledgements. We thank Prof. M. Kiya, Department of Engineering, Hokkaido University, for his introduction to fluid dynamics. We wish to thank three unknown referees for the critical comments on the early version of this manuscript. This work was supported by a Grant-in-Aid for Scientific Research, 56440006, from the Japanese Ministry of Education, Science and Culture.

References

Chapman KM, Smith RS (1963) A linear transfer function underlying impulse frequency modulation in a cockroach mechanoreceptor. Nature 197:699–700

Dagan D, Camhi JM (1979) Responses to wind recorded from the cercal nerve of the cockroach *Periplaneta americana*. II. Directional selectivity of the sensory neurons innervating single columns of filiform hairs. J Comp Physiol 133:103–110

Dumpert K, Gnatzy W (1977) Cricket combined mechanoreceptors and kicking response. J Comp Physiol 122:9–25

Fletcher NH (1978) Acoustical response of hair receptors in insects. J Comp Physiol 127:185–189

Gnatzy W, Romer F (1980) Morphogenesis of mechanoreceptor and epidermal cells of crickets during the last instar, and its relation to molting-hormone level. Cell Tissue Res 213:369–391

Gnatzy W, Tautz J (1980) Ultrastructure and mechanical properties of an insect mechanoreceptor: Stimulus-transmitting structures and sensory apparatus of the cercal filiform hairs of *Gryllus*. Cell Tissue Res 213:441–463

Henson BL, Wilkens LA (1979) A mathematical model for the motion of mechanoreceptor hairs in fluid environments. Biophys J 27:277–286

Imai I (1980) Oseen's method for two dimensional flow. In: Fluid dynamics. vol. 1. Syokabo, Tokyo pp 388–395

Jensen M, Weiss-Fogh T (1962) Biology and physics of locust flight V. Strength and elasticity of locust cuticle. Phil Trans R Soc Lond B 245:137–163 (cited in Tautz J 1977)

Kanou M, Shimozawa T (1984) A threshold analysis of cricket cercal interneurons by an alternating air-current stimulus. J Comp Physiol A 154:357–365

Lawrence PA (1966) Development and determination of hairs and bristles in the milkweed bug, *Oncopeltus fasciatus* (Lygaeidae, Hemiptera). J Cell Sci 1:475–498

Nicklaus R (1965) Die Erregung einzelner Fadenhaare von *Periplaneta americana* in Abhängigkeit von der Größe und Richtung der Auslenkung. Z Vergl Physiol 50:331–362

Petrovskaya YD, Rozhkova GI, Tokareva VS (1970) Characteristics of single receptors of the cercal auditory system of the house cricket. Biofizika 15:1112–1119 (English version)

Schlichting H (1979) Exact solutions of the Navier-Stokes equations. In: Boundary layer theory. McGraw-Hill, New York pp 83–112

Shimozawa T, Kanou M (1984) Varieties of filiform hairs: range fractionation by sensory afferents and cercal interneurons of a cricket. J Comp Physiol A 155:485–493

Takahata M (1981) Functional differentiation of crayfish statocyst receptors in sensory adaptation. Comp Biochem Physiol 68 A:17–23

Tautz J (1977) Reception of medium vibration by thoracal hairs of caterpillars of *Barathra brassicae* L. (Lepidoptera, Noctuidae). I. Mechanical properties of the receptor hairs. J Comp Physiol 118:13–31

Tautz J (1979) Reception of particle oscillation in a medium. An unorthodox sensory capacity. Naturwissenschaften 66:452–461